Journal of Sound and Vibration (2002) **255**(3), 579–602
doi:10.1006/jsvi.2001.4161, available online at http://www.idealibrary.com on IDEAL®

VIBRATION CHARACTERISTICS AND TRANSIENT RESPONSE OF SHEAR-DEFORMABLE FUNCTIONALLY GRADED PLATES IN THERMAL ENVIRONMENTS

J. YANG

School of Civil Engineering and Mechanics, Shanghai Jiao Tong University, 1954 *Hua Shan Road, Shanghai* 200030, *People's Republic of China*; *and Department of Mechanical Engineering, Wuhan Institute of Chemical Technology, Wuhan 430073, People's Republic of China*

AND

H.-S. SHEN

School of Civil Engineering and Mechanics, Shanghai Jiao Tong University, 1954 *Hua Shan Road, Shanghai* 200030, *People's Republic of China. E-mail*: *hsshen@mail.sjtu.edu.cn*

(*Received* 9 *July* 2001, *and in final form* 21 *November* 2001)

Free and forced vibration analyses for initially stressed functionally graded plates in thermal environment are presented. Material properties are assumed to be temperature dependent, and graded in the thickness direction according to a simple power law distribution in terms of the volume fractions of the constituents. Theoretical formulations are based on Reddy's higher order shear deformation plate theory and include the thermal effects due to uniform temperature variation. The plate is assumed to be clamped on two opposite edges with the remaining two others either free, simply supported or clamped. One-dimensional differential quadrature technique, Galerkin approach, and the modal superposition method are used to determine the transient response of the plate subjected to lateral dynamic loads. Comprehensive numerical results for silicon nitride/stainless-steel rectangular plates are presented in dimensionless tabular and graphical forms. The roles played by the constituent volume fraction index, temperature rise, shape and duration of dynamic loads, initial membrane stresses as well as the character of boundary conditions are studied. The results reveal that, when thermal effects are considered, functionally graded plates with material properties intermediate to those of isotropic ones do not necessarily have intermediate natural frequencies and dynamic responses.

1. INTRODUCTION

Functionally graded materials (FGMs) are usually made from a mixture of metals and ceramics through powder metallurgy processes. They have been regarded as one of the advanced inhomogeneous composite materials in many engineering sectors due to their flexible properties that can be tailored to different applications and working environments [1, 2]. This can be achieved by gradually varying the volume fraction of constituent materials so that the mechanical properties exhibit a smooth and continuous change from one surface to the other. FGMs have now been developed as important structural components mainly used in high-temperature conditions and have been receiving considerably more attention in recent years.

Numerous studies on free and forced vibration for isotropic and composite multilayered plates with or without initial thermal and/or mechanical in-plane loads have been reported,

0022-460X/02/$35.00

see, for example, references [3–14]. However, investigations on the free vibration and transient response of FGM structures are limited in number. Among those, Tanigawa *et al.* [15] examined transient thermal stress distribution of FGM plates induced by unsteady heat conduction. Reddy and Chin [16] discussed a wide range of problems in FGM cylinders and plates including thermo-mechanical coupling effects, among which transient response of the plate due to heat flux was one of the topics addressed. Finite element solutions were given for simply supported rectangular plates by using the first order shear deformation plate theory (FSDPT). Loy *et al.* [17] presented Rayleigh–Ritz solutions for free vibration of simply supported FGM cylindrical shells. Gong *et al.* [18] investigated the transient response of FGM cylindrical shells under low-velocity impact. He *et al.* [19] gave finite element formulations for the shape and vibration control of FGM thin plates with integrated piezoelectric sensors and actuators. In references [17–19], material properties were considered as a function of temperature, but the results were only for a fixed temperature environment. Praveen and Reddy [20], also based on FSDPT, analyzed the non-linear static and dynamic response of functionally graded ceramic–metal plates in a steady temperature field and subjected to lateral dynamic loads by the finite element method. Reddy [21] developed both theoretical and finite element formulations for thick FGM plates according to the higher order shear deformation plate theory, and studied the non-linear dynamic response of FGM plates subjected to suddenly applied uniform pressure. However, they assumed that the material properties were temperature independent. It should also be noted that none of the aforementioned analyses [15–21] considered the effect of initial membrane stresses. To the best of authors' knowledge, there are no results in the open literature concerning the vibration as well as transient response of shear deformable FGM plates subjected to lateral dynamic load combined with initial in-plane actions and in thermal environments. This is the subject of the present work.

In this paper, we assume that the functionally graded plates are made from two constituent materials, whose material properties are non-linear functions of temperature and graded in the thickness direction according to a power-law distribution of material composition. The plate may be initially stressed by in-plane actions and has two opposite edges clamped with the remaining two others either free, simply supported or clamped. Both movable and immovable in-plane boundary conditions are considered. Reddy's higher order shear deformation plate theory (HSDPT) [22] is used to predict the dynamic response of FGM plates due to arbitrary dynamic loading. A semi-analytical approach is then developed, which makes use of differential quadrature approximation, Galerkin technique, and the modal superposition method. Comprehensive numerical results for the natural frequencies and dynamic response of silicon nitride/stainless-steel rectangular plates are presented. A parametric study is also carried out, highlighting the effects of material composition, initial thermal and/or mechanical in-plane loads on the transient response characteristics. The numerical results presented herein for FGM plates are not available in the literature, and therefore, should be of interest to the engineering community.

2. THEORETICAL FORMULATIONS

2.1. FGM MATERIAL PROPERTIES

Here we consider an FGM rectangular plate of length a, width b and thickness h, which is made from a mixture of ceramics and metals. We assume that the composition is varied from the top to the bottom surface, i.e., the top surface ($Z = h/2$) of the plate is ceramic-rich, whereas the bottom surface ($Z = -h/2$) is metal-rich. In such a way, the effective material

properties P, such as Young's modulus E, the Poisson ratio v, mass density ρ, and coefficient of thermal expansion α can be expressed as

$$P = P_t V_c + P_b V_m, \tag{1}$$

where subscripts "t" and "b" refer to the top and bottom surfaces of the plate, respectively; V_c and V_m are the ceramic and metal volume fractions and are related by

$$V_c + V_m = 1. \tag{2}$$

The ceramic volume fraction V_c is assumed to follow a simple power distribution as [16]

$$V_c = \left(\frac{2Z + h}{2h}\right)^n, \tag{3}$$

where volume fraction index n dictates the material variation profile through the plate thickness and may be varied to obtain the optimum distribution of component materials. From equations (1)–(3), the effective Young's modulus E, the Poisson ratio v, mass density ρ and thermal expansion coefficient α of an FGM plate can be written as

$$E = (E_t - E_b)\left(\frac{2Z + h}{2h}\right)^n + E_b, \tag{4a}$$

$$v = (v_t - v_b)\left(\frac{2Z + h}{2h}\right)^n + v_b, \tag{4b}$$

$$\rho = (\rho_t - \rho_b)\left(\frac{2Z + h}{2h}\right)^n + \rho_b, \tag{4c}$$

$$\alpha = (\alpha_t - \alpha_b)\left(\frac{2Z + h}{2h}\right)^n + \alpha_b. \tag{4d}$$

For functionally graded materials in high operating temperature, significant variations in thermal and mechanical properties of the materials are to be expected. Accurate prediction of the mechanical response requires accounting for this temperature dependency. Therefore, E_t, E_b, v_t, v_b, ρ_t, ρ_b, α_t and α_b are functions of temperature, as will be shown in section 4, so that E, v, ρ and α are both temperature and position dependent.

Thermal force resultants, thermal moment resultants and higher order thermal moment resultants due to temperature rise ΔT are defined by

$$\begin{bmatrix} \bar{N}_X^T & \bar{M}_X^T & \bar{P}_X^T \\ \bar{N}_Y^T & \bar{M}_Y^T & \bar{P}_Y^T \\ \bar{N}_{XY}^T & \bar{M}_{XY}^T & \bar{P}_{XY}^T \end{bmatrix} = \int_{-h/2}^{h/2} \begin{bmatrix} A_X \\ A_Y \\ A_{XY} \end{bmatrix} (1, Z, Z^3)\, \Delta T \, \mathrm{d}Z, \tag{5}$$

where

$$\begin{bmatrix} A_X \\ A_Y \\ A_{XY} \end{bmatrix} = -\begin{bmatrix} Q_{11} & Q_{12} & Q_{16} \\ Q_{12} & Q_{22} & Q_{26} \\ Q_{16} & Q_{26} & Q_{66} \end{bmatrix} \begin{bmatrix} 1 & 0 \\ 0 & 1 \\ 0 & 0 \end{bmatrix} \begin{bmatrix} \alpha \\ \alpha \end{bmatrix} \tag{6}$$

and

$$Q_{11} = Q_{22} = \frac{E}{1-\nu^2}, \quad Q_{12} = \frac{\nu E}{1-\nu^2}, \quad Q_{16} = Q_{26} = 0, \quad Q_{44} = Q_{55} = Q_{66} = \frac{E}{2(1+\nu)}. \tag{7}$$

The various plate inertias may be calculated by

$$(I_1, I_2, I_3, I_4, I_5, I_7) = \int_{-h/2}^{h/2} \left\{(\rho_t - \rho_b)\left(\frac{2Z+h}{2h}\right)^n + \rho_b\right\}(1, Z, Z^2, Z^3, Z^4, Z^6)\,\mathrm{d}Z. \tag{8}$$

2.2. GOVERNING EQUATIONS

Suppose the plate is initially stress free at temperature T_0, and is then subjected to thermo-mechanical loads, which include a uniform temperature rise ΔT, a uniform lateral dynamic load $q(X, Y, \bar{t})$ combined with in-plane edge loads p_X in X direction and p_Y in Y direction.

Let $\bar{t}$ be time, Ω be the natural frequency of the plate, $\bar{U}$, $\bar{V}$ and $\bar{W}$ be the plate displacements parallel to a right-hand set of co-ordinates (X, Y, Z), $\bar{\Psi}_X$ and $\bar{\Psi}_Y$ be the mid-plane rotations of transverse normals about the Y- and X-axis respectively. By introducing the stress function $\bar{F}(X, Y)$ for the stress resultants ($\bar{N}_X = \bar{F}_{,YY}$, $\bar{N}_Y = \bar{F}_{,XX}$ and $\bar{N}_{XY} = -\bar{F}_{,XY}$), the equations of motion for an FGM rectangular plate can be derived as follows:

$$\tilde{L}_{11}(\bar{W}) - \tilde{L}_{12}(\bar{\Psi}_X) - \tilde{L}_{13}(\bar{\Psi}_Y) + \tilde{L}_{14}(\bar{F}) - \tilde{L}_{15}(\bar{N}^{\mathrm{T}}) - \tilde{L}_{16}(\bar{M}^{\mathrm{T}}) = q - \tilde{L}_{17}(\ddot{\bar{W}}) - \hat{I}_5\left(\frac{\partial \ddot{\bar{\Psi}}_X}{\partial X} + \frac{\partial \ddot{\bar{\Psi}}_Y}{\partial Y}\right), \tag{9}$$

$$\tilde{L}_{21}(\bar{F}) + \tilde{L}_{22}(\bar{\Psi}_X) + \tilde{L}_{23}(\bar{\Psi}_Y) - \tilde{L}_{24}(\bar{W}) - \tilde{L}_{25}(\bar{N}^T) = 0, \tag{10}$$

$$\tilde{L}_{31}(\bar{W}) + \tilde{L}_{32}(\bar{\Psi}_X) - \tilde{L}_{33}(\Psi_Y) + \tilde{L}_{34}(\bar{F}) - \tilde{L}_{35}(\bar{N}^{\mathrm{T}}) - \tilde{L}_{36}(\bar{S}^{\mathrm{T}}) = -I_3'\ddot{\bar{\Psi}}_X + I_5'\frac{\partial \ddot{\bar{W}}}{\partial X}, \tag{11}$$

$$\tilde{L}_{41}(\bar{W}) - \tilde{L}_{42}(\bar{\Psi}_X) + \tilde{L}_{43}(\bar{\Psi}_Y) + \tilde{L}_{44}(\bar{F}) - \tilde{L}_{45}(\bar{N}^{\mathrm{T}}) - \tilde{L}_{46}(\bar{S}^{\mathrm{T}}) = -I_3'\ddot{\bar{\Psi}}_Y + I_5'\frac{\partial \ddot{\bar{W}}}{\partial Y}, \tag{12}$$

where the operators $\tilde{L}_{11}(\ )$ and $\tilde{L}_{17}(\ )$ are defined as

$$\tilde{L}_{11}(\ ) = c_1\left[F_{11}^*\frac{\partial^4}{\partial X^4} + (F_{12}^* + F_{21}^* + 4F_{66}^*)\frac{\partial^4}{\partial X^2 \partial Y^2} + F_{22}^*\frac{\partial^4}{\partial Y^4}\right] - \left(p_X\frac{\partial^2 \bar{W}}{\partial X^2} + p_Y\frac{\partial^2 \bar{W}}{\partial Y^2}\right),$$

$$\tilde{L}_{17}(\ ) = I_1 + \hat{I}_7\left(\frac{\partial^2}{\partial X^2} + \frac{\partial^2}{\partial Y^2}\right) \tag{13}$$

and all other operators are defined as in reference [23], and

$$I_3' = I_3 - 2c_1 I_5 + c_1^2 I_7 - (I_2 - c_1 I_4)^2/I_1, \tag{14a}$$

$$I_5' = c_1[I_5 - c_1 I_7 - I_4(I_2 - c_1 I_4)/I_1], \tag{14b}$$

$$I_7' = c_1^2(I_4^2/I_1 - I_7), \qquad \hat{I}_5 = I_3' + I_5', \quad \hat{I}_7 = I_7' - I_5'. \tag{14c–e}$$

In the above equations $c_1 = 4/3h^2$, $\bar{S}^T = \bar{M}^T - c_1 \bar{P}^T$, and the reduced stiffness matrices $[A_{ij}^*]$, $[B_{ij}^*]$, $[D_{ij}^*]$, $[E_{ij}^*]$, $[F_{ij}^*]$, $[H_{ij}^*]$ $(i, j = 1, 2, 6)$ are determined through relationship [23, 24]

$$\mathbf{A}^* = \mathbf{A}^{-1}, \qquad \mathbf{B}^* = -\mathbf{A}^{-1}\mathbf{B}, \qquad \mathbf{D}^* = \mathbf{D} - \mathbf{B}\mathbf{A}^{-1}\mathbf{B}, \qquad \mathbf{E}^* = -\mathbf{A}^{-1}\mathbf{E},$$
$$\mathbf{F}^* = \mathbf{F} - \mathbf{E}\mathbf{A}^{-1}\mathbf{B}, \qquad \mathbf{H}^* = \mathbf{H} - \mathbf{E}\mathbf{A}^{-1}\mathbf{E}, \tag{15}$$

in which

$$(A_{ij}, B_{ij}, D_{ij}, E_{ij}, F_{ij}, H_{ij}) = \int_{-h/2}^{h/2} Q_{ij}(1, Z, Z^2, Z^3, Z^4, Z^6)\,\mathrm{d}Z \quad (i, j = 1, 2, 6), \tag{16a}$$

$$(A_{ij}, D_{ij}, F_{ij}) = \int_{-h/2}^{h/2} Q_{ij}(1, Z^2, Z^4)\,\mathrm{d}Z \quad (i, j = 4, 5). \tag{16b}$$

It is noted that, because of equation (5), $\tilde{L}_{15}(N^T) = \tilde{L}_{25}(N^T) = \tilde{L}_{35}(N^T) = \tilde{L}_{45}(N^T) = 0$.

The plate is assumed to be clamped on two opposite edges (at $Y = 0, b$) and the remaining two edges may be free, simply supported or clamped, so that the boundary conditions are

$X = 0, a$:

Simply supported (S):

$$\bar{W} = \bar{\Psi}_Y = \bar{M}_X = \bar{P}_X = \bar{N}_{XY} = 0, \tag{17a}$$

$$\int_0^b \bar{N}_X\,dY + p_X b = 0 \text{ (movable) or } \bar{U} = 0 \text{ (immovable).} \tag{17b}$$

Clamped (C):

$$\bar{W} = \bar{\Psi}_X = \bar{\Psi}_Y = \frac{\partial \bar{W}}{\partial X} = \bar{N}_{XY} = 0, \tag{17c}$$

$$\int_0^b \bar{N}_X\,\mathrm{d}Y + p_X b = 0 \text{ (movable) or } \bar{U} = 0 \text{ (immovable).} \tag{17d}$$

Free (F):

$$\bar{M}_X = \bar{P}_X = \bar{M}_{XY} - c_1 \bar{P}_{XY} = \bar{Q}_X - c_2 \bar{R}_X - c_1\left(\frac{\partial \bar{P}_X}{\partial X} + 2\frac{\partial \bar{P}_{XY}}{\partial Y}\right) = \bar{N}_{XY} = 0, \tag{17e}$$

$$\int_0^b \bar{N}_X\,\mathrm{d}Y + p_X b = 0. \tag{17f}$$

$Y = 0, b$:

$$\bar{W} = \bar{\Psi}_X = \bar{\Psi}_Y = \frac{\partial \bar{W}}{\partial Y} = \bar{N}_{XY} = 0, \tag{18a}$$

$$\int_0^a \bar{N}_Y\,\mathrm{d}X + p_Y a = 0 \text{ (movable)} \quad \text{or} \quad \bar{V} = 0 \text{ (immovable)}, \tag{18b}$$

where $\bar{M}_X$, $\bar{M}_{XY}$ denote the bending moments per unit width of the plate, $\bar{Q}_X$ is the transverse shear force, $\bar{P}_X$, $\bar{P}_{XY}$ and $\bar{R}_X$ are the higher order moment and shear force.

Definition of these stress resultants was given in reference [22] and will not be repeated here for brevity.

Following Shen [24], the immovable in-plane boundary conditions are fulfilled on the average sense as

$$\int_0^b \int_0^a \frac{\partial \bar{U}}{\partial X}\,\mathrm{d}X\,dY = 0 \quad \text{at } X = 0,\, a \qquad \int_0^a \int_0^b \frac{\partial \bar{V}}{\partial Y}\,\mathrm{d}Y\,\mathrm{d}X = 0 \quad \text{at } Y = 0,\, b. \tag{19a, b}$$

The average end-shortening relationships are

$$\begin{aligned}\frac{\Delta_X}{a} &= -\frac{1}{ab}\int_0^b \int_0^a \frac{\partial \bar{U}}{\partial X}\,\mathrm{d}X\,\mathrm{d}Y \\ &= -\frac{1}{ab}\int_0^b \int_0^a \left\{\left[A_{11}^* \frac{\partial^2 \bar{F}}{\partial Y^2} + A_{12}^* \frac{\partial^2 \bar{F}}{\partial X^2} + (B_{11}^* - c_1 E_{11}^*)\frac{\partial \bar{\Psi}_X}{\partial X} + (B_{12}^* - c_1^* E_{12}^*)\frac{\partial \bar{\Psi}_Y}{\partial Y}\right.\right. \\ &\quad \left.\left. - c_1\left(E_{11}^* \frac{\partial^2 \bar{W}}{\partial X^2} + E_{12}^* \frac{\partial^2 \bar{W}}{\partial Y^2}\right)\right] - (A_{11}^* \bar{N}_X^{\mathrm{T}} + A_{12}^* \bar{N}_Y^{\mathrm{T}})\right\}\mathrm{d}X\,\mathrm{d}Y, \end{aligned} \tag{20a}$$

$$\begin{aligned}\frac{\Delta_Y}{b} &= -\frac{1}{ab}\int_0^b \int_0^a \frac{\partial \bar{V}}{\partial Y}\,\mathrm{d}X\,\mathrm{d}Y \\ &= -\frac{1}{ab}\int_0^b \int_0^a \left\{\left[A_{22}^* \frac{\partial^2 \bar{F}}{\partial X^2} + A_{12}^* \frac{\partial^2 \bar{F}}{\partial Y^2} + (B_{21}^* - c_1 E_{21}^*)\frac{\partial \bar{\Psi}_X}{\partial X} + (B_{22}^* - c_1 E_{22}^*)\frac{\partial \bar{\Psi}_Y}{\partial Y}\right.\right. \\ &\quad \left.\left. - c_1\left(E_{21}^* \frac{\partial^2 \bar{W}}{\partial X^2} + E_{22}^* \frac{\partial^2 \bar{W}}{\partial Y^2}\right)\right] - (A_{12}^* \bar{N}_X^{\mathrm{T}} + A_{22}^* \bar{N}_Y^{\mathrm{T}})\right\}\mathrm{d}X\,\mathrm{d}Y. \end{aligned} \tag{20b}$$

The following dimensionless quantities are introduced:

$$x = X/a, \qquad y = Y/b, \qquad \beta = a/b, \qquad t = \bar{t}\sqrt{D_{11}^*/I_1}/a^2, \qquad \omega = \Omega a^2\sqrt{I_1/D_{11}^*},$$

$$\Delta = (D_{11}^* D_{22}^* A_{11}^* A_{22}^*)^{1/4}, \qquad W = \bar{W}/\Delta, \qquad F = \bar{F}/(D_{11}^* D_{22}^*)^{1/2}, \qquad (\Psi_x, \Psi_y) = (\bar{\Psi}_X, \bar{\Psi}_Y)\,a/\Delta,$$

$$\lambda_q = qa^4/D_{11}^*\Delta, \qquad \gamma_{14} = [D_{22}^*/D_{11}^*]^{1/2}, \qquad \gamma_{24} = [A_{11}^*/A_{22}^*]^{1/2}, \qquad \gamma_5 = -A_{12}^*/A_{22}^*,$$

$$(\gamma_{T1}, \gamma_{T2}) = (A_X^{\mathrm{T}}, A_Y^{\mathrm{T}})\,a^2/(D_{11}^* D_{22}^*)^{1/2},$$

$$(M_x, M_y, M_x^{\mathrm{T}}, M_y^{\mathrm{T}}) = (\bar{M}_X, \bar{M}_Y, \bar{M}_X^{\mathrm{T}}, \bar{M}_Y^{\mathrm{T}})\,a^2/D_{11}^*\Delta,$$

$$(P_x, P_y, P_x^{\mathrm{T}}, P_y^{\mathrm{T}}) = c_1(\bar{P}_X, \bar{P}_Y, \bar{P}_X^{\mathrm{T}}, \bar{P}_Y^{\mathrm{T}})\,a^2/D_{11}^*\Delta, \qquad (I_3^*, I_5^*, I_7^*) = (I_3', I_5', I_7')/a^2 I_1,$$

$$(\lambda_x, \lambda_y) = (p_X b^2, p_Y a^2)/(D_{11}^* D_{22}^*)^{1/2}, \qquad (\delta_x, \delta_y) = (\Delta_X/a, \Delta_Y/b)\,b^2/\Delta, \tag{21}$$

where $A_X^{\mathrm{T}}(= A_Y^{\mathrm{T}})$ are defined by

$$\begin{bmatrix} A_X^{\mathrm{T}} \\ A_Y^{\mathrm{T}} \end{bmatrix} = -\int_{-h/2}^{h/2} \begin{bmatrix} A_X \\ A_Y \end{bmatrix} \mathrm{d}Z. \tag{22}$$

Equations of motion (9–12) can then be written in dimensionless form as

$$L_{11}(W) - L_{12}(\Psi_x) - L_{13}(\Psi_y) + \gamma_{14}L_{14}(F) - L_{16}(M^{\mathrm{T}}) = \lambda_q - L_{17}(\ddot{W}) - \hat{I}_5^*\left(\frac{\partial \ddot{\Psi}_x}{\partial x} + \frac{\partial \ddot{\Psi}_y}{\partial y}\right), \tag{23}$$

$$L_{21}(F) + \gamma_{24}L_{22}(\Psi_x) + \gamma_{24}L_{23}(\Psi_y) - \gamma_{24}L_{24}(W) = 0, \tag{24}$$

$$L_{31}(W) + L_{32}(\Psi_x) - L_{33}(\Psi_y) + \gamma_{14}L_{34}(F) - L_{36}(S^{\mathrm{T}}) = -I_3^*\ddot{\Psi}_x + I_5^*\frac{\partial \ddot{W}}{\partial x}, \tag{25}$$

$$L_{41}(W) - L_{42}(\Psi_x) + L_{43}(\Psi_y) + \gamma_{14}L_{44}(F) - L_{46}(S^{\mathrm{T}}) = -I_3^*\ddot{\Psi}_y + I_5^*\frac{\partial \ddot{W}}{\partial y}, \tag{26}$$

where $\hat{I}_5^* = I_3^* + I_5^*, \hat{I}_7^* = I_7^* - I_5^*$, and

$$L_{11}(\ ) = \gamma_{110}\frac{\partial^4}{\partial x^4} + 2\gamma_{112}\beta^2\frac{\partial^4}{\partial x^2\partial y^2} + \gamma_{114}\beta^4\frac{\partial^4}{\partial y^4} - \gamma_{14}\beta^2\left(\lambda_x\frac{\partial^2 W}{\partial x^2} + \lambda_y\frac{\partial^2 W}{\partial y^2}\right),$$

$$L_{12}(\ ) = \gamma_{120}\frac{\partial^3}{\partial x^3} + \gamma_{122}\beta^2\frac{\partial^3}{\partial x\partial y^2},$$

$$L_{13}(\ ) = \gamma_{131}\beta\frac{\partial^3}{\partial x^2\partial y} + \gamma_{133}\beta^3\frac{\partial^3}{\partial y^3},$$

$$L_{14}(\ ) = \gamma_{140}\frac{\partial^4}{\partial x^4} + \gamma_{142}\beta^2\frac{\partial^4}{\partial x^2\partial y^2} + \gamma_{144}\frac{\partial^4}{\partial y^4},$$

$$L_{16}(M^{\mathrm{T}}) = \frac{\partial^2}{\partial x^2}(M_x^{\mathrm{T}}) + 2\beta\frac{\partial^2}{\partial x\partial y}(M_{xy}^{\mathrm{T}}) + \beta^2\frac{\partial^2}{\partial y^2}(M_y^{\mathrm{T}}),$$

$$L_{17}(\ ) = 1 - \hat{I}_7^*\left(\frac{\partial^2}{\partial x^2} + \beta^2\frac{\partial^2}{\partial y^2}\right),$$

$$L_{21}(\ ) = \frac{\partial^4}{\partial x^4} + \gamma_{212}\beta^2\frac{\partial^4}{\partial x^2\partial y^2} + \gamma_{214}\beta^4\frac{\partial^4}{\partial y^4},$$

$$L_{22}(\ ) = \gamma_{220}\frac{\partial^3}{\partial x^3} + \gamma_{222}\beta^2\frac{\partial^3}{\partial x\partial y^2}, \quad L_{23}(\ ) = \gamma_{231}\beta\frac{\partial^3}{\partial x^2\partial y} + \gamma_{233}\beta^3\frac{\partial^3}{\partial y^3},$$

$$L_{24}(\ ) = \gamma_{240}\frac{\partial^4}{\partial x^4} + \gamma_{242}\beta^2\frac{\partial^4}{\partial x^2\partial y^2} + \gamma_{244}\beta^4\frac{\partial^4}{\partial y^4},$$

$$L_{31}(\ ) = \gamma_{31}\frac{\partial}{\partial x} + \gamma_{310}\frac{\partial^3}{\partial x^3} + \gamma_{312}\beta^2\frac{\partial^3}{\partial x\partial y^2},$$

$$L_{32}(\ ) = \gamma_{31} - \gamma_{320}\frac{\partial^2}{\partial x^2} - \gamma_{322}\beta^2\frac{\partial^2}{\partial y^2},$$

$$L_{33}(\ ) = \gamma_{331}\beta\frac{\partial^2}{\partial x\partial y},\quad L_{34}(\ ) = L_{22}(\ ),\quad L_{36}(S^{\mathrm{T}}) = \frac{\partial}{\partial x}(S_x^{\mathrm{T}}) + \beta\frac{\partial}{\partial y}(S_{xy}^{\mathrm{T}}),$$

$$L_{41}(\ ) = \gamma_{41}\beta\frac{\partial}{\partial y} + \gamma_{411}\beta\frac{\partial^3}{\partial x^2\partial y} + \gamma_{413}\beta^3\frac{\partial^3}{\partial y^3},\quad L_{42}(\ ) = L_{33}(\ ),$$

$$L_{43}(\ ) = \gamma_{41} - \gamma_{430}\frac{\partial^2}{\partial x^2} - \gamma_{432}\beta^2\frac{\partial^2}{\partial y^2},\quad L_{44}(\ ) = L_{23}(\ ),$$

$$L_{46}(S^{\mathrm{T}}) = \frac{\partial}{\partial x}(S_{xy}^{\mathrm{T}}) + \beta\frac{\partial}{\partial y}(S_y^{\mathrm{T}}). \tag{27}$$

The boundary conditions of equations (17) and (18) become

$x = 0,\ 1$:

Simply supported (S):

$$W = \Psi_y = M_x = P_x = \frac{\partial^2 F}{\partial x\partial y} = 0, \tag{28a}$$

$$\int_0^1 \frac{\partial^2 F}{\partial y^2}\,\mathrm{d}y + \lambda_x = 0 \text{ (movable)} \quad \text{or} \quad \delta_x = 0 \text{ (immovable)}. \tag{28b}$$

Clamped (C):

$$W = \Psi_x = \Psi_y = \frac{\partial W}{\partial x} = \frac{\partial^2 F}{\partial x\partial y} = 0, \tag{28c}$$

$$\int_0^1 \frac{\partial^2 F}{\partial y^2}\,\mathrm{d}y + \lambda_x = 0 \text{ (movable)} \quad \text{or} \quad \delta_x = 0 \text{ (immovable)}. \tag{28d}$$

Free (F):

$$M_x = P_x = M_{xy} - c_1 P_{xy} = Q_x - c_2 R_x - c_1\left(\frac{\partial P_x}{\partial x} + 2\beta\frac{\partial P_{xy}}{\partial y}\right) = \frac{\partial^2 F}{\partial x\partial y} = 0, \tag{28e}$$

$$\int_0^1 \frac{\partial^2 F}{\partial y^2}\,\mathrm{d}y + \lambda_x = 0. \tag{28f}$$

$y = 0,\ 1$:

$$W = \Psi_x = \Psi_y = \frac{\partial W}{\partial y} = \frac{\partial^2 F}{\partial x\partial y} = 0, \tag{29a}$$

$$\int_0^1 \frac{\partial^2 F}{\partial x^2}\,\mathrm{d}x + \lambda_y = 0 \text{ (movable)} \quad \text{or} \quad \delta_y = 0 \text{ (immovable)} \tag{29b}$$

and the end-shortening relationships become

$$\delta_x = -\frac{1}{\gamma_{24}\beta^2}\int_0^1\int_0^1\left\{\left[\gamma_{24}^2\beta^2\frac{\partial^2 F}{\partial y^2} - \gamma_5\frac{\partial^2 F}{\partial x^2} + \gamma_{24}\left(\gamma_{511}\frac{\partial \Psi_x}{\partial x} + \gamma_{233}\beta\frac{\partial \Psi_x}{\partial y}\right)\right.\right.$$
$$\left.\left. - \gamma_{24}\left(\gamma_{611}\frac{\partial^2 W}{\partial x^2} + \gamma_{244}\beta^2\frac{\partial^2 W}{\partial y^2}\right)\right] + (\gamma_{24}^2\gamma_{T1} - \gamma_5\gamma_{T2})\,\Delta T\right\}\mathrm{d}x\,\mathrm{d}y, \tag{30a}$$

$$\delta_y = -\frac{1}{\gamma_{24}\beta^2}\int_0^1\int_0^1\left\{\left[\frac{\partial^2 F}{\partial x^2} - \gamma_5\beta^2\frac{\partial^2 F}{\partial y^2} + \gamma_{24}\left(\gamma_{220}\frac{\partial \Psi_x}{\partial x} + \gamma_{522}\beta\frac{\partial \Psi_x}{\partial y}\right)\right.\right.$$
$$\left.\left. - \gamma_{24}\left(\gamma_{240}\frac{\partial^2 W}{\partial x^2} + \gamma_{622}\beta^2\frac{\partial^2 W}{\partial y^2}\right)\right] + (\gamma_{T2} - \gamma_5\gamma_{T1})\,\Delta T\right\}\mathrm{d}x\,\mathrm{d}y. \tag{30b}$$

In equations (27) and (30), all other dimensionless quantities γ_{ijk} are defined as in references [23, 24] and will not be repeated here for the sake of brevity.

3. SOLUTION METHODOLOGY

3.1. SEMI-ANALYTICAL DIFFERENTIAL QUADRATURE METHOD

This section extends our previous work [25, 26] to predict the transient response of FGM rectangular plates. Solutions of W, Ψ_x, Ψ_y and F are constructed as

$$W = \sum_{m=1}^{M} a_m(t)w_m(x,y), \qquad \Psi_x = \sum_{m=1}^{M} b_m(t)\psi_{xm}(x,y) \tag{31a, b}$$

$$\Psi_y = \sum_{m=1}^{M} c_m(t)\psi_{ym}(x,y) \tag{31c}$$

$$F = -\tfrac{1}{2}(y^2\lambda_x + x^2\lambda_y) + \sum_{m=1}^{M} d_m(t)f_m(x,y). \tag{31d}$$

According to differential quadrature technique, w_m, ψ_{xm}, ψ_{ym} and f_m are approximated along x-axis in terms of their function values at a number of pre-selected sampling points by

$$\{w_m, \psi_{xm}, \psi_{ym}, f_m\} = \sum_{j=1}^{N} l_j(x)\{w_{jm}, \psi_{xjm}, \psi_{yjm}, f_{jm}\}, \tag{32}$$

where $l_j(x)$ is the Lagrange interpolation polynomial, and $w_{jm} = w_m(x_j, y)$, $\psi_{xjm} = \psi_{xm}(x_j, y)$, $\psi_{yjm} = \psi_{ym}(x_j, y)$, $f_{jm} = f_m(x_j, y)$. Further, their rth partial derivatives with respect to x at a sampling point x_i $(i = 1, \ldots, N)$ are expressed as

$$\frac{\partial^r}{\partial x^r}\{w_m, \psi_{xm}, \psi_{ym}, f_m\}|_{x=x_i} = \sum_{j=1}^{N} C_{ij}^{(r)}\{w_{jm}, \psi_{xjm}, \psi_{yjm}, f_{jm}\}. \tag{33}$$

Recursive formula for weighting coefficient $C_{ij}^{(r)}$ is available in reference [27]. Its value depends on the choice of the interpolation function and the sampling point system, which in

the present analysis is designed as

$$x_1 = 0{\cdot}0, \quad x_2 = 0{\cdot}0001, \quad x_j = \frac{1}{2}\left[1 - \cos\frac{\pi(j-2)}{N-3}\right], \quad x_{N-1} = 0{\cdot}9999, \quad x_N = 1{\cdot}0. \tag{34}$$

For the plate clamped at $y = 0,1$, w_{jm}, ψ_{xjm}, ψ_{yjm} and f_{jm} are modelled by

$$w_{jm} = \sin\alpha_m y - \sinh\alpha_m y - \xi_m(\cos\alpha_m y - \cosh\alpha_m y), \tag{35a}$$

$$f_{jm} = \sin\alpha_m y - \sinh\alpha_m y - \xi_m(\cos\alpha_m y - \cosh\alpha_m y), \tag{35b}$$

$$\psi_{xjm} = \sin(m\pi y), \quad \psi_{yjm} = \sin(m\pi y), \tag{35c}$$

where

$$\xi_m = (\sin\alpha_m - \sinh\alpha_m)/(\cos\alpha_m - \cosh\alpha_m), \quad \alpha_m = (2m+1)\pi/2. \tag{35d}$$

It should be pointed out that, although our present work focuses on initially stressed FGM plates clamped at $y = 0$, 1, it is equally applicable to deal with FGM plates simply supported at $y = 0$, 1 only if initial in-plane actions are absent and w_{jm}, ψ_{xjm}, ψ_{yjm} and f_{jm} are assumed as

$$w_{jm} = \sin(m\pi y), \tag{36a}$$

$$f_{jm} = \sin\alpha_m y - \sinh\alpha_m y - \xi_m(\cos\alpha_m y - \cosh\alpha_m y), \tag{36b}$$

$$\psi_{xjm} = \sin(m\pi y), \quad \psi_{yjm} = \cos(m\pi y). \tag{36c}$$

Application of equations (31–33) to the equations of motion (23–26) produces $4N$ sets of ordinary differential equations. Finally, substituting equation (35) or (36) into these equations and then applying the Galerkin procedure leads to

$$[\mathbf{K}]\{\boldsymbol{\delta}(t)\} + [\mathbf{G}]\{\ddot{\delta}(t)\} = \{\mathbf{R}(t)\}, \tag{37}$$

where $[\mathbf{K}]$ and $[\mathbf{G}]$ are constant matrices, $\{\mathbf{R}(t)\}$ is the dynamic load vector, $\{\boldsymbol{\delta}(t)\}$ is a column vector comprising of $a_{jm}(t)$, $b_{jm}(t)$, $c_{jm}(t)$ and $d_{jm}(t)$ at each nodal line.

If, in equation (37), the lateral load vector $\{\mathbf{R}(t)\}$ vanishes, a linear eigenvalue problem is then produced, from which vibration characteristics of the FGM plate can be readily determined

$$([\mathbf{K}] - \omega^2[\mathbf{G}])\{\boldsymbol{\delta}\} = \{0\}. \tag{38}$$

3.2. MODAL SUPERPOSITION APPROACH FOR TRANSIENT RESPONSE

Now we try to solve equation (37) and assume that

$$\{\boldsymbol{\delta}(t)\} = \sum_{k=1} \{\boldsymbol{\delta}^{(k)}\} T^{(k)}(t) \tag{39}$$

in which $T^{(k)}(t)$ is the kth order principal modal co-ordinate, and $\boldsymbol{\delta}^{(k)}$ is the modal shape function associated with the kth order natural frequency parameter $\omega^{(k)}$. Substituting

TABLE 1

Temperature-dependent coefficients of elastic modulus E (GPa), the Poisson ratio v, mass density $\rho(kg/m^3)$ and linear thermal expansion $\alpha(1/K)$ ceramics and metals (from reference [16])

	Material	P_{-1}	P_0	P_1	P_2	P_3
E	Si_3N_4	0	348·43e9	−3·070e − 4	2·160e-7	−8·946e − 11
	SUS304	0	201·04e9	3·079e − 4	−6·534e − 7	0
	Ti–6Al–4V	0	122·56e9	−4·586e − 4	0	0
	Aluminum oxide	0	349·55e9	−3·853e − 4	4·027e − 7	−1·673e − 10
v	Si_3N_4	0	0·2400	0	0	0
	SUS304	0	0·3262	−2.002e − 4	3.797e − 7	0
	Ti–6Al–4V	0	0·2884	1.121e − 4	0	0
	Aluminum oxide	0	0·26	0	0	0
ρ	Si_3N_4	0	2370	0	0	0
	SUS304	0	8166	0	0	0
	Ti–6Al–4V	0	4429	0	0	0
	Aluminum oxide	0	3750	0	0	0
α	Si_3N_4	0	5.8723e − 6	9.095e − 4	0	0
	SUS304	0	12.330e − 6	8.086e − 4	0	0
	Ti–6Al–4V	0	7.5788e − 6	6.638e − 4	−3.147e − 6	0
	Aluminum oxide	0	6.8269e − 6	1·838e − 4	0	0

equation (39) into equation (37), we get

$$\sum_{k=1} ([\mathbf{K}]\{\boldsymbol{\delta}^{(k)}\}\, T^{(k)}(t) + [\mathbf{G}]\{\boldsymbol{\delta}^{(k)}\}\, \ddot{T}^{(k)}(t)) = \{\mathbf{R}(t)\}. \tag{40}$$

Making use of orthogonality properties of the modal shape functions yields

$$\ddot{T}^{(k)}(t) + (\omega^{(k)})^2\, T^{(k)}(t) = R^{(k)}(t)/G^{(k)} \tag{41}$$

in which

$$R^{(k)}(t) = \{\boldsymbol{\delta}^{(k)}\}^{\mathrm{T}}\{\mathbf{R}(t)\}, \qquad G^{(k)} = \{\boldsymbol{\delta}^{(k)}\}^{\mathrm{T}}[\mathbf{G}]\{\boldsymbol{\delta}^{(k)}\}. \tag{42}$$

If zero-valued initial conditions prevail, the solution of equation (41) can be obtained as

$$T^{(k)}(t) = \frac{1}{\omega^{(k)} G^{(k)}} \int_0^t R^{(k)}(\tau) \sin[\omega^{(k)}(t-\tau)\, \mathrm{d}\tau. \tag{43}$$

Re-substituting $T^{(k)}(t)$ into equation (39) yields a transient response at any given time.

4. NUMERICAL RESULTS AND DISCUSSION

This section consists of three parts: (1) accuracy and convergence studies of present formulations; (2) free vibration analysis with comprehensive information on the natural frequency parameters of FGM rectangular plates; and (3) numerical results for the transient response of FGM rectangular plates. Silicon nitride and stainless steel are chosen to be the

TABLE 2

Natural frequencies (Hz) of simply supported aluminum oxide/Ti–6Al–4V square plates

Source	Mode sequence									
$n = 0$	1	2	3	4	5	6	7	8	9	10
$N \times M = 9 \times 5$	143·99	360·10	360·10	569·44	699·36	719·81	918·77	918·77	1281·31	1791·33
$N \times M = 11 \times 5$	143·96	360·06	360·06	568·85	718·55	718·22	916·76	916·76	1207·13	1221·67
$N \times M = 13 \times 5$	143·96	360·07	360·07	568·87	718·22	718·22	916·40	916·40	1207·13	1207·13
$N \times M = 15 \times 6$	143·96	360·07	360·07	568·88	718·22	718·22	916·40	916·40	1207·09	1207·09
He *et al.* [19]	144·66	360·53	360·53	569·89	720·57	720·57	919·74	919·74	1225·72	1225·72
$n = 2000$										
$N \times M = 9 \times 5$	261·50	653·18	654·04	1045·31	1261·77	1304·79	1672·90	1696·09	2214·41	2312·21
$N \times M = 11 \times 5$	261·46	653·10	653·10	1044·27	1303·60	1303·60	1693·83	1694·94	2214·41	2269·67
$N \times M = 13 \times 5$	261·46	653·13	653·13	1044·30	1304·79	1304·79	1694·98	1694·98	2214·41	2214·41
$N \times M = 15 \times 6$	261·46	653·14	653·14	1044·31	1304·79	1304·79	1694·98	1694·98	2214·34	2214·34
He *et al.* [19]	268·92	669·40	669·40	1052·49	1338·52	1338·52	1695·23	1695·23	2280·95	2280·98

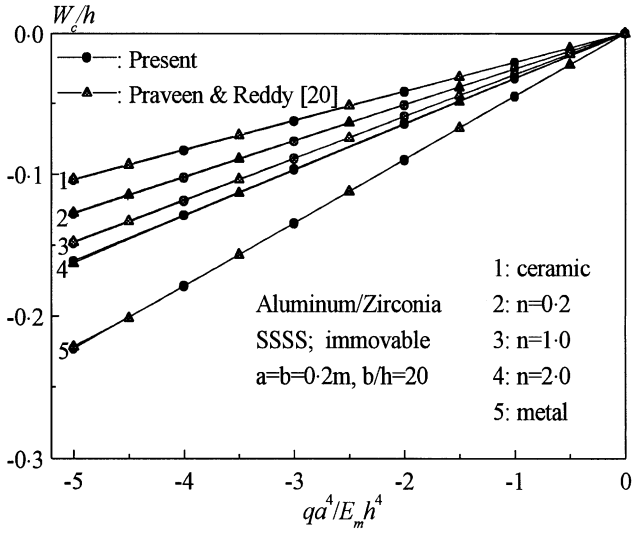

Figure 1. Comparisons of dimensionless central deflection versus load for SSSS FGM square plates under uniform lateral pressure.

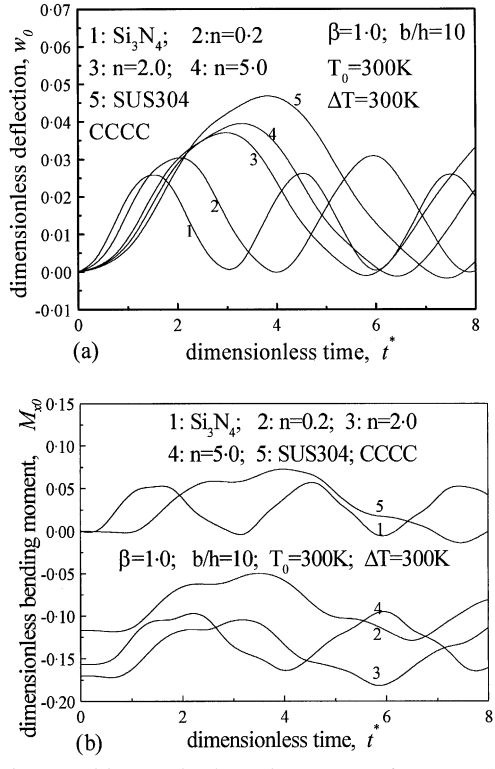

Figure 2. Effect of material composition on the dynamic response of CCCC FGM square plates subjected to a suddenly applied lateral load: (a) central deflection versus time; (b) central bending moment versus time.

constituent materials of the FGM plate, referred to as Si_3N_4/SUS304, in the present analysis. Their material properties P, such as Young's modulus E, the Poisson ratio ν, coefficient of thermal expansion α and mass density ρ can be expressed as a non-linear

TABLE 3

Frequency parameter $\omega^* = (\Omega b^2/\pi^2)\sqrt{I_0/D_0}$ *for initially stressed CCCC FGM square plates* ($b/h = 10$, $T_0 = 300\,\mathrm{K}$, $\Delta T = 300$, *movable edges*)

(λ_x, λ_y)	Material composition	Mode sequences							
		1	2	3	4	5	6	7	8
Without in-plane load									
(0, 0)	Si_3N_4	7·2881	14·0406	14·0406	19·9234	22·3000	23·5294	27·4326	28·5645
	$n = 0{\cdot}2$	5·6087	10·8110	10·8110	15·3407	17·0530	18·1203	21·0162	21·9918
	$n = 2{\cdot}0$	3·9680	7·6201	7·6201	10·7972	12·1600	12·7314	14·9223	15·4456
	$n = 5{\cdot}0$	3·6104	6·9116	6·9116	9·7777	11·0655	11·5138	13·5468	13·9563
	$n = 10{\cdot}0$	3·4832	6·6610	6·6610	9·4180	10·6792	11·0853	13·0622	13·4329
	SUS304	3·1703	6·0764	6·0764	8·5985	9·6632	10·1307	11·8541	12·2786
Under uniaxial in-plane loads									
(0, −5)	Si_3N_4	8·9507	14·9389	17·4802	22·3730	24·0521	26·9978	30·2916	31·3337
	$n = 0{\cdot}2$	6·8833	11·4980	13·4452	17·2119	18·5196	20·6879	23·3074	24·0241
	$n = 2{\cdot}0$	4·8841	8·1184	9·5244	12·1599	13·0229	14·7428	16·4127	17·0761
	$n = 5{\cdot}0$	4·4521	7·3715	8·6657	11·0367	11·7833	13·4302	14·8534	15·5244
	$n = 10{\cdot}0$	4·2980	7·1068	8·3601	10·6388	11·3467	12·9642	14·3039	14·9750
	SUS304	3·9050	6·4762	7·6041	9·6913	10·3646	11·7401	13·0542	13·5842
(0, 5)	Si_3N_4	4·9417	9·6267	13·0631	15·8552	17·1023	22·6390	22·9755	24·1620
	$n = 0{\cdot}2$	3·8156	7·4414	10·0643	11·9073	13·1883	17·2554	17·6977	18·1990
	$n = 2{\cdot}0$	2·6655	5·1597	7·0763	8·6897	9·2216	12·3076	12·4212	13·2759
	$n = 5{\cdot}0$	2·4061	4·6319	6·4084	7·9372	8·3173	11·1660	11·2254	12·1914
	$n = 10{\cdot}0$	2·3149	4·4481	6·1727	7·6751	8·0003	10·7669	10·8050	11·8306
	SUS304	2·1239	4·0997	5·6399	6·8394	7·3334	9·7404	9·8817	10·4131
Under biaxial in-plane loads									
(−5, −5)	Si_3N_4	10·3562	18·0354	18·0354	24·4867	27·4436	28·2317	32·8375	33·6531
	$n = 0{\cdot}2$	7·9634	13·8711	13·8711	18·8288	21·0303	21·7116	25·1754	25·8714
	$n = 2{\cdot}0$	5·6546	9·8269	9·8269	13·3304	14·9883	15·3474	17·9095	18·2868
	$n = 5{\cdot}0$	5·1573	8·9417	8·9417	12·1147	13·6549	13·9304	16·2918	16·5864
	$n = 10{\cdot}0$	4·9797	8·6266	8·6266	11·6828	13·1813	13·4284	15·7181	15·9847
	SUS304	4·5226	7·8456	7·8456	10·6291	11·9368	12·2277	14·2520	14·5556
(5, 5)	Si_3N_4	4·1264	8·0910	8·0910	13·8397	15·0218	17·5560	20·3600	22·2890
	$n = 0{\cdot}2$	3·5310	6·2684	6·2684	10·7029	11·2573	13·5674	15·5005	17·2184
	$n = 2{\cdot}0$	3·0857	4·2971	4·2971	7·3903	8·2294	9·3830	11·0399	11·9147
	$n = 5{\cdot}0$	2·1872	3·8272	3·8272	6·6123	7·5132	8·4022	9·9946	10·6675
	$n = 10{\cdot}0$	2·0820	3·6652	3·6652	6·3428	7·2645	8·0625	9·6316	10·2354
	SUS304	1·8524	3·4201	3·4201	5·8607	6·4662	7·4406	8·7179	9·4426

function of temperature, see reference [28], as

$$P = P_0(P_{-1}T^{-1} + 1 + P_1T + P_2T^2 + P_3T^3) \tag{44}$$

in which $T = T_0 + \Delta T$ and $T_0 = 300\,\mathrm{K}$ (room temperature), P_0, P_{-1}, P_1, P_2 and P_3 are the coefficients of temperature $T(\mathrm{K})$ and are unique to the constituent materials. Typical values for silicon nitride and stainless steel are listed in Table 1 (from reference [16]).

A uniform lateral dynamic pressure $q(X, Y, \bar{t}) = q_0F(\bar{t})$ is applied on the top surface of the plate, in which q_0 is the maximum amplitude and $F(\bar{t})$ is a dynamic load shape function in time domain. Three sets of lateral loads, namely, suddenly applied load (Case 1),

TABLE 4

Frequency parameter $\omega^* = (\Omega b^2/\pi^2)\sqrt{I_0 D_0}$ *for FGM rectangular plates with immovable inplane constraints on all edges* ($\lambda_x = 0$, $\lambda_y = 0$, $b/h = 10$, $T_0 = 300\,\mathrm{K}$, $\Delta T = 300\,\mathrm{K}$)

Boundary condition	β	n	Mode sequences							
			1	2	3	4	5	6	7	8
CCCC	0·5	0·2	13·2966	16·8384	21·7947	29·5710	29·9195	30·4560	32·4340	36·4854
		2·0	9·2196	11·6913	15·2957	20·4667	21·2323	21·4468	22·4853	25·4461
		10·0	7·9839	10·1219	13·3088	17·6295	18·3727	18·9066	19·3778	21·9914
	1·0	0·2	5·2968	10·4371	10·4371	14·9290	16·5741	17·7034	20·5278	21·5468
		2·0	3·6638	7·2545	7·2545	10·3924	11·7056	12·3207	14·4521	15·0049
		10·0	3·1835	6·3001	6·3001	9·0171	10·2372	10·6781	12·6015	12·9948
	1·5	0·2	3·9765	6·1040	9·5486	9·5486	11·3705	14·0829	14·3854	15·7688
		2·0	2·7373	4·2236	6·6331	6·6331	7·9088	9·8122	10·0191	11·1492
		10·0	2·3753	3·6692	5·7618	5·7618	6·8690	8·5206	8·6979	9·7598
CSCC	0·5	0·2	10·4436	14·9271	20·5267	26·3159	29·2684	29·5666	29·7938	34·2248
		2·0	7·2700	10·3909	14·4520	18·3203	20·6030	20·7767	21·0353	23·9649
		10·0	6·3045	9·0158	12·6007	15·8335	17·8142	17·9830	18·5759	20·7626
	1·0	0·2	4·6631	9·1716	10·2161	14·1166	16·1116	16·4120	19·9868	19·9868
		2·0	3·2130	6·3768	7·1005	9·8347	11·2403	11·5963	14·0890	14·0890
		10·0	2·7875	5·5432	6·1677	8·5402	9·7597	10·1457	12·2956	12·2956
	1·5	0·2	3·7925	5·5711	8·7758	9·4673	11·0884	13·0969	13·8702	15·7197
		2·0	2·6055	3·8464	6·0993	6·5763	7·7126	9·1348	9·6646	11·1159
		10·0	2·2589	3·3394	5·3034	5·7124	6·6996	7·9411	8·3942	9·7315
CSCS	0·5	0·2	8·0435	13·3985	19·5039	22·9349	26·9062	28·7000	29·0742	32·0506
		2·0	5·6274	9·3391	13·7657	16·0523	18·8195	20·3041	20·6723	22·5310
		10·0	4·8601	8·1143	12·0203	13·9352	16·3154	17·5880	18·2817	19·5699
	1·0	0·2	4·2154	8·0126	9·9887	13·3987	14·5651	16·2614	19·2150	19·5020
		2·0	2·8949	5·5639	6·9416	9·3387	10·1822	11·4954	13·4275	13·7617
		10·0	2·5069	4·8386	6·0299	8·1141	8·8554	10·0600	11·6601	12·0190
	1·5	0·2	3·6645	5·1178	8·0131	9·4005	10·8442	12·1363	13·3988	15·6765
		2·0	2·5148	3·5238	5·5646	6·5295	7·5421	8·4704	9·3387	11·0866
		10·0	2·1791	3·0565	4·8389	5·6718	6·5521	7·3709	8·1141	9·7065

sinusoidal load (Case 2), and exponential load (Case 3), are considered in the present analysis, whose pulse shapes are defined as

Case 1:

$$F(\bar{t}) = 1. \tag{45a}$$

Case 2:

$$F(\bar{t}) = \begin{cases} \sin(\pi \bar{t}/\bar{t}_0), & \bar{t} \leqslant \bar{t}_0, \\ 0, & \bar{t} > \bar{t}_0. \end{cases} \tag{45b}$$

Case 3:

$$F(\bar{t}) = \mathrm{e}^{-\xi \bar{t}}. \tag{45c}$$

In the following numerical illustrations, the initial stress-free temperature is set at $T_0 = 300$ K. D_0 and I_0 are chosen to be the values of D_{11} and I_1 of a stainless-steel plate of

TABLE 5

Frequency parameter $\omega^* = (\Omega b^2/\pi^2)\sqrt{I_0 D_0}$ *for FGM square plates under three sets of thermal environments* ($n = 2{\cdot}0$, $T_0 = 300\,\mathrm{K}$, *immovable*)

ΔT (K)	Boundary condition	b/h	Mode sequences							
			1	2	3	4	5	6	7	8
0	CCCC	10	4·1062	7·8902	7·8902	11·1834	12·5881	13·1867	15·4530	16·0017
		5	6·8757	12·1576	12·1576	16·5854	18·9362	19·2780	22·5928	22·7898
	CSCC	10	3·6705	7·0131	7·7426	10·6189	12·0942	12·4766	15·0828	15·1834
		5	6·2670	11·2265	12·0465	16·0202	17·9957	19·1341	21·8714	22·4638
	CSCS	10	3·3564	6·2058	7·5814	10·1160	11·0243	12·3740	14·3955	14·7487
		5	5·7918	10·2959	11·8412	15·4864	17·0128	19·0295	21·1590	22·1571
300	CCCC	10	3·6636	7·2544	7·2544	10·3924	11·7054	12·3175	14·4520	15·0019
		5	6·4638	11·4980	11·4980	15·7253	17·9744	18·3085	21·4681	21·6633
	CSCC	10	3·2130	6·3768	7·1005	9·8347	11·2403	11·5963	14·0890	14·2002
		5	5·8653	10·5940	11·3852	15·1786	17·0657	18·1691	20·7717	21·3492
	CSCS	10	2·8949	5·5639	6·9416	9·3387	10·1822	11·4954	13·4275	13·7617
		5	5·4004	9·6876	11·1862	14·6624	16·1151	18·0682	20·0842	21·0538
500	CCCC	10	3·2357	6·6281	6·6281	9·5990	10·8285	11·4350	13·4412	13·9756
		5	6·0369	10·7959	10·7959	14·7982	16·9321	17·2601	20·2414	20·4373
	CSCC	10	2·7712	5·7598	6·4707	9·0547	10·3862	10·7235	13·0899	13·2002
		5	5·4556	9·9297	10·6839	14·2760	16·0647	17·1274	19·5771	20·1384
	CSCS	10	2·4499	4·9479	6·3157	8·5709	9·3539	10·6255	12·4519	12·7736
		5	5·0067	9·0575	10·4933	13·7829	15·1583	17·0315	18·9217	19·8575

$b/h = 10$. E_0 and ρ_0 serve, respectively, as the reference values of elastic modulus and mass density, and are selected to be the Young's modulus and mass density of stainless steel. The above reference parameters are all evaluated at T_0. Dimensionless in-plane loads are expressed as $(\lambda_x, \lambda_y) = (p_x, p_y)a^2/\pi^2 D_{11}^*$. For the sake of brevity, a clockwise notation starting from $y = 0$ is employed. Symbol "CSCF", for example, identifies a plate clamped at $y = 0$, 1, simply supported at $x = 0$, and free at $x = 1$. A program was developed for the purpose and many examples were solved numerically, including the following.

4.1. CONVERGENCE AND ACCURACY STUDIES

To validate the present method for FGM plates, two test examples are first examined. By varying the number of N and M, convergence study has been undertaken in Table 2 for the first 10 natural frequencies of simply supported aluminum oxide/Ti–6Al–4V square plates ($a = b = 0{\cdot}4\,\mathrm{m}$, $h = 0{\cdot}005\,\mathrm{m}$, $n = 0$, 2000) together with the solutions given by He *et al.* [19] for direct comparison. The plates are purely aluminum oxide at the top surface and purely Ti–6Al–4V at the bottom surface with the material properties evaluated at $T_0 = 300\,\mathrm{K}$. It is observed that the present method converges well enough to obtain results in good agreement with those in reference [19], when $N \geqslant 13$ and $M \geqslant 5$. Thus, $N \times M = 13 \times 5$ has been used in all the following computations.

As another part of validation, static bending of simply supported aluminum/zirconia square plates ($a \times b \times h = 0{\cdot}2\,\mathrm{m} \times 0{\cdot}2\,\mathrm{m} \times 0{\cdot}01\,\mathrm{m}$) under uniform lateral pressure is considered. Results are compared in Figure 1 with the finite element solutions of Praveen

TABLE 6

Frequency parameter $\omega^* = (\Omega b^2/\pi^2)\sqrt{I_0 D_0}$ *for FGM square plates having free edge(s) at* $x = 0$ *and/or* 1 *and immovable constraints at* $y = 0, 1$ ($\lambda_x = 0$, $\lambda_y = 0$, $n = 2{\cdot}0$, $T_0 = 300\,\mathrm{K}$)

ΔT (K)	Boundary condition	b/h	Mode sequences							
			1	2	3	4	5	6	7	8
0	CCCF	10	2·7939	4·5380	6·9679	8·3109	8·6828	11·8089	12·0395	13·4111
		5	4·8453	7·5422	10·9235	13·0657	13·3379	17·8871	18·1978	20·0965
	CSCF	10	2·7342	4·0710	6·9364	7·4410	8·3963	11·4629	11·7852	12·6117
		5	4·7422	6·9144	10·8773	12·1021	13·0115	17·2953	18·1726	19·1323
	CFCF	10	2·6040	3·0576	4·9221	6·7622	7·3815	8·7630	9·3925	11·6084
		5	4·5404	5·2263	8·2485	10·6181	11·5263	13·9973	14·3996	17·9293
300	CCCF	10	2·5382	4·2903	6·4864	7·9788	8·1917	11·1014	11·4873	12·6845
		5	4·5849	7·2213	10·3821	12·5715	12·7370	17·1537	17·3552	19·3437
	CSCF	10	2·4773	3·8289	6·4553	7·1343	7·9097	10·9254	11·0783	12·1487
		5	4·4842	6·6121	10·3376	11·6442	12·4209	16·5830	17·3312	18·4299
	CFCF	10	2·3420	2·8072	4·6683	6·2807	6·8960	8·4183	8·8879	10·9029
		5	4·2857	4·9570	7·9084	10·0844	10·9669	13·4772	13·7671	17·0946
500	CCCF	10	2·2929	4·0328	6·0081	7·6050	7·6830	10·3901	10·8847	11·9330
		5	4·3098	6·8602	9·7950	11·9949	12·0669	16·3131	16·4287	18·3906
	CSCF	10	2·2317	3·5822	5·9778	6·7930	7·4089	10·3428	10·3675	11·6120
		5	4·2129	6·2753	9·7527	11·1121	11·7643	15·7685	16·4059	17·6013
	CFCF	10	2·0929	2·5621	4·3996	5·8054	6·4057	8·0275	8·3553	10·1962
		5	4·0206	4·6664	7·5214	9·5084	10·3526	12·8685	13·0531	16·1787

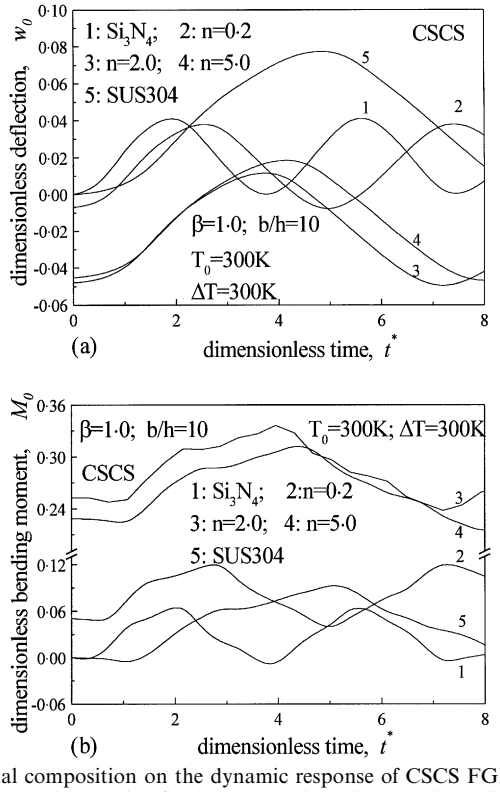

Figure 3. Effect of material composition on the dynamic response of CSCS FGM square plates subjected to a suddenly applied lateral load: (a) central deflection versus time; (b) central bending moment versus time.

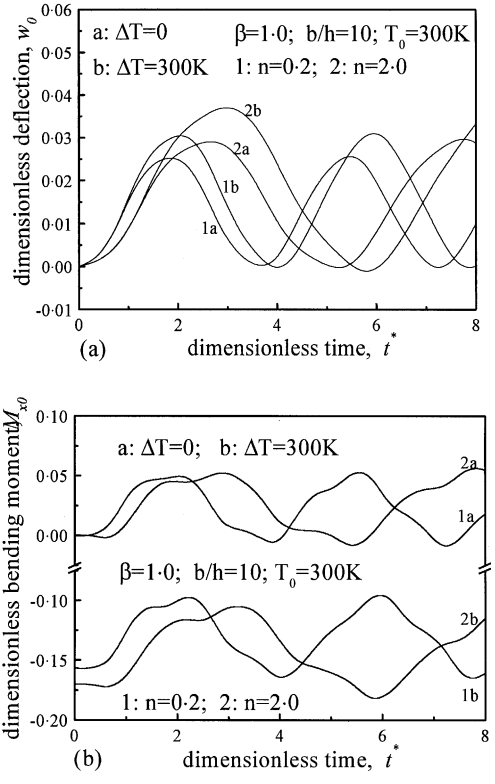

Figure 4. Effect of temperature rise ΔT on the dynamic response of CCCC FGM plates subjected to a suddenly applied lateral load: (a) central deflection versus time; (b) central bending moment versus time.

and Reddy [20]. In this comparison the material properties are assumed to be temperature-independent, i.e., $E_m = 70$ GPa, $v_m = 0{\cdot}3$, $E_c = 151$ GPa, $v_c = 0{\cdot}3$. They show that the present results agree well with those in reference [20].

4.2. NUMERICAL RESULTS FOR FREE VIBRATION

Dimensionless natural frequency parameters $\omega^* = (\Omega b^2/\pi^2)\sqrt{I_0/D_0}$ of Si_3N_4/SUS304 rectangular plates are given in a tabular form. Table 3 gives the natural frequencies of pre-stressed CCCC FGM square plates ($b/h = 10$) with different material compositions and under thermal environmental condition $\Delta T = 300$ K. In Table 3, movable in-plane boundary conditions are considered. The fully Si_3N_4 and SUS304 cases correspond to isotropic plates in nature, while the other four cases ($n = 0{\cdot}2$, 2, 5, 10) are for the graded plates with two constituent materials. It is evident that, from Table 1, the bending stiffness is the maximum for the ceramic plate, the minimum for the metallic plate, and degrades gradually as the volume fraction index n increases. Five sets of initial in-plane loading conditions are considered. $\lambda_x = \lambda_y = 0$ denotes no in-plane loads. $\lambda_x = 0$ and $\lambda_y = -5$ (or 5) denote unixial stretching or compression, and $\lambda_x = \lambda_y = -5$ (or 5) denotes equal biaxial stretching or compression. As demonstrated by the results, ω^* decreases as material composition varies from pure silicon nitride to pure steel. It is also observed that, for the fixed material mixtures, with the same increase in temperature, ω^* increases by increasing initial in-plane tension and decreases by increasing initial edge compression.

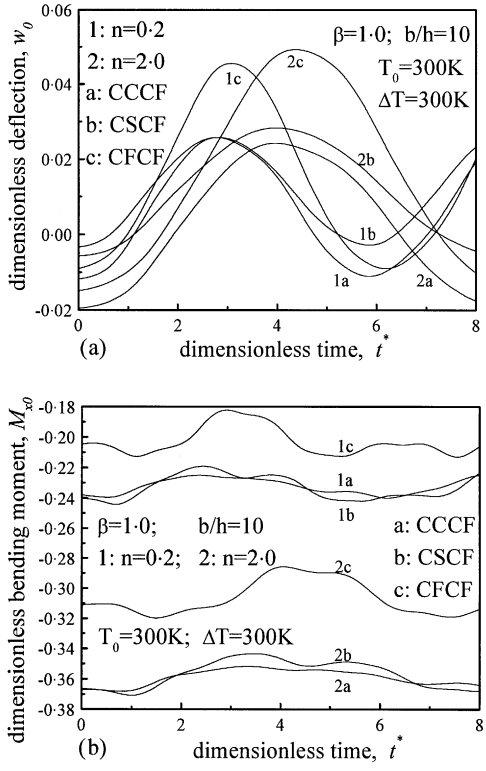

Figure 5. Effect of free boundary condition on the dynamic response of FGM square plates with immovable edges at $Y = 0$, b and subjected to a suddenly applied lateral load: (a) central deflection versus time; (b) central bending moment versus time.

Table 4 gives frequencies of FGM rectangular plates ($\beta = 0{\cdot}5$, $1{\cdot}0$, $1{\cdot}5$) with volume fraction index n ($= 0{\cdot}2$, 2, 10) and with different boundary conditions (CSCS, CSCC and CCCC), under thermal environmental condition $\Delta T = 300$ K. Immovable in-plane boundary conditions are considered. The results show that the CCCC rectangular plate has the highest, whereas the CSCS plate has the lowest natural frequency values, implying that the plate with greater support rigidity will have higher vibrating frequencies. Meanwhile, ω^* decreases dramatically as β increases from 0·5 to 1·5, and decrease as n increases from 0·2 to 10.

To show the effects of thermal environments, transverse shear deformation and rotary inertia on vibration characteristics of FGM plates, dimensionless frequencies for CCCC, CSCC and CSCS FGM square plates ($n = 2{\cdot}0$) with different values of b/h (= 5, 10) are given in Table 5. Three sets of thermal environments, i.e., $\Delta T = 0$, 300 and 500 K are taken into consideration. As expected, ω^* decreases as ΔT increases. This is because Young's modulus usually decreases with rising temperatures. It can be seen that, due to the effects of transverse shear deformation and rotary inertia, the frequencies of FGM plates increase as b/h varies from 10 to 5.

In Table 6, we examine the vibration characteristics of an FGM square plate ($n = 2{\cdot}0$) with immovable edges at $y = 0$, 1 and free edge(s) at $x = 0$ and/or 1. The results show that the CCCF plate has the maximum value, and the CFCF plate has the minimum value of ω^*.

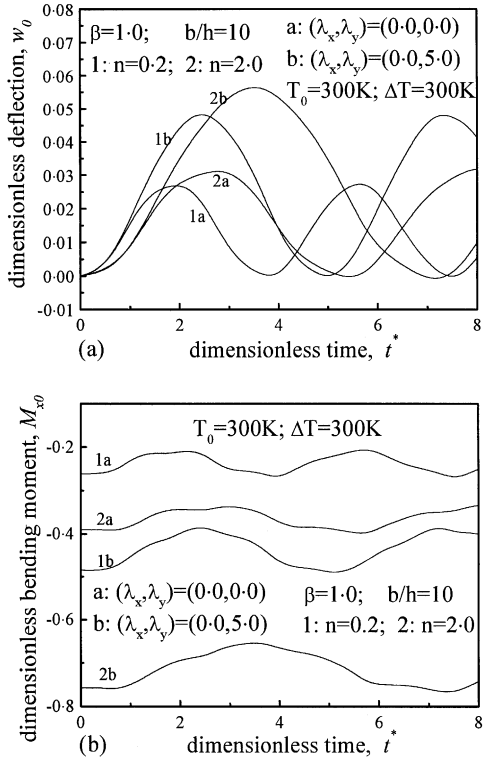

Figure 6. Effect of initial membrane stress on the dynamic response of CCCC FGM square plates subjected to a suddenly applied lateral load: (a) central deflection versus time; (b) central bending moment versus time.

4.3. NUMERICAL RESULTS FOR TRANSIENT RESPONSE

Parametric studies have been performed to study the transient response of FGM plates subjected to a uniform lateral dynamic load combined with initial membrane stresses under thermal environments. Typical results are plotted in Figures 2–8. It should be appreciated that in all these figures, $t^* = \bar{t}\sqrt{E_0/\rho_0 a^2}$, $w_0 = \bar{W}_c E_0 h^3/q_0 a^4$ and $M_{x0} = \bar{M}_{Xc}/q_0 a^2$ represent the dimensionless forms of, respectively, time, deflection and bending moment at the point $(X, Y) = (a/2, b/2)$.

We begin by examining the effect of material composition on the transient response of CCCC and CSCS Si_3N_4/SUS304 square plates subjected to a suddenly applied lateral load, under thermal environmental condition $\Delta T = 300$ K. Figures 2 and 3 show, respectively, the deflections and bending moments as functions of varying volume fraction index n. For the CCCC plate, the higher the bending rigidity is, the lower will be the peak value of deflections. However, the minimum dynamic deflection of the CSCS plate occurs when $n = 0{\cdot}2$, but not in the case of an isotropic silicon nitride plate, indicating that the dynamic response of graded plates do not necessarily lie between those of isotropic metal and ceramic plates.

It is noted that, in both Figures 2 and 3, bending moments of plates with graded material composition are much higher than those of purely metallic and ceramic plates. This is due to the fact that, the thermal expansion at the top surface is lower than that at the bottom surface, uniform high temperature change results in a downward deflection and initial bending moments of the FGM plate.

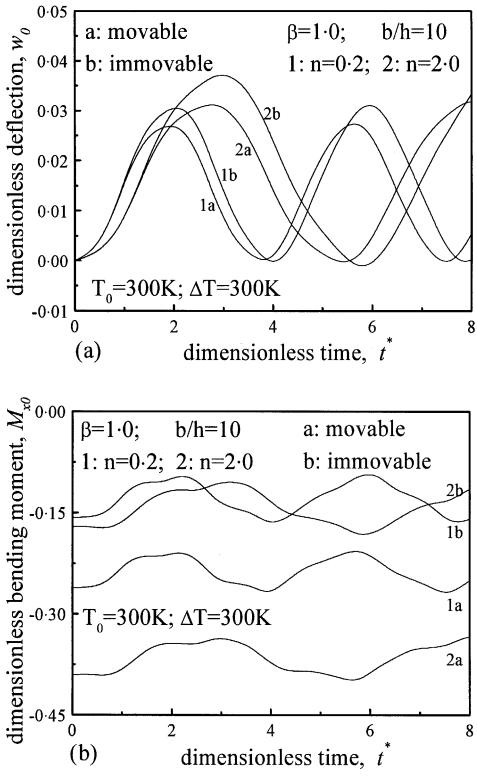

Figure 7. Effect of in-plane boundary constraints on the dynamic response of CCCC FGM square plates subjected to a suddenly applied lateral load: (a) central deflection versus time; (b) central bending moment versus time.

Figure 4 shows the effect of thermal environments on the dynamic response of a CCCC FGM rectangular plate subjected to a suddenly applied lateral load, under thermal environmental conditions $\Delta T = 0$ and 300 K. It can be seen that both deflections and bending moments increase dramatically with increasing ΔT.

Figure 5 gives the dimensionless central deflection and bending moment as functions of time for FGM square plates with free edge(s) at $x = 0$ and/or 1 (CFCF, CCCF and CSCF). Results show that the plate with two opposite free edges, namely, the CFCF plate, produces much more deflections and much less bending moments than the CCCF and CSCF plates. It is also observed that the greater the volume fraction index n is, the greater will be the thermally induced initial bending moments, and the plates with free edge will have more bending moments than those without free edges.

Figure 6 shows the effects of initial membrane stresses on the dynamic response of a CCCC FGM square plate with movable in-plane boundary conditions, subjected to a suddenly applied lateral load and under thermal environmental condition $\Delta T = 300$ K. The results reveal that, although no initial deflections are induced by membrane stresses, application of in-plane compression will result in considerable increase in both deflections and bending moments.

Figure 7 compares the dynamic response of CCCC FGM square plates with movable and immovable in-plane boundary conditions under the same loading condition of Figure 6. It is seen that both dynamic deflection and bending moment in an immovable CCCC plate are greater than those in a movable CCCC plate.

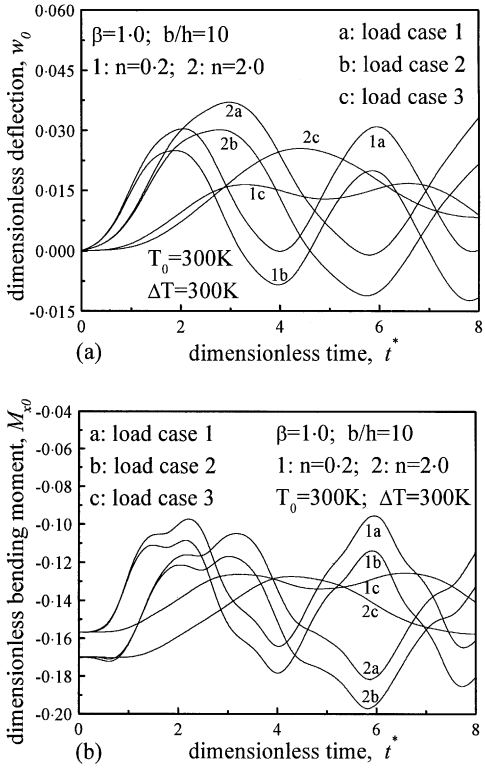

Figure 8. Effect of dynamic load shape on the dynamic response of CCCC FGM square plates under thermal environments: (a) central deflection versus time; (b) central bending moment versus time.

Figure 8 compares the dynamic response of a CCCC FGM square plate under load cases 1–3, i.e., suddenly applied load, sinusoidal load and exponential load, as defined in equation (45). Here, the values used in the computations are dimensionless duration of the load $\bar{t}_0\sqrt{E_0/\rho_0 h} = 6$ and $\xi = 4$.

In Figures 4–8, the volume fraction index is chosen to be $n = 0{\cdot}2$ and $2{\cdot}0$, and in Figures 2–4 and 8, all the results are for the FGM plate with immovable in-plane boundary conditions on all edges.

5. CONCLUDING REMARKS

Free vibration and the dynamic response of functionally graded rectangular plates subjected to impulsive lateral loads combined with initial in-plane actions and under thermal environments are investigated by using a semi-analytical approach. The present formulations are based on Reddy's higher order shear deformation plate theory to account for the rotary inertia and parabolic distribution of the transverse shear strains through the plate thickness. Non-linear temperature-dependency of material properties is also taken into account. The plate under consideration is clamped on two opposite edges and may be either free, simply supported or clamped on the remaining two others. Natural frequency parameters and dynamic response for silicon nitride/stainless-steel rectangular plates are presented in tabular and graphical format respectively. Numerical results show that, when thermal effects are included, the plates with intermediate material properties do not

necessarily have intermediate dynamic response. They also confirm that the vibration characteristics and dynamic responses are significantly influenced by material composition, temperature rise, the character of in-plane and out-of-plane boundary conditions, initial membrane stresses, as well as dynamic load shape.

ACKNOWLEDGMENT

This work is supported in part by the National Natural Science Foundation of China under Grant 59975058. The authors are grateful for this financial support.

REFERENCES

1. M. YAMANOUCHI, M. KOIZUMI, T. HIRAI and I. SHIOTA (editors) 1990 *Proceedings of the* 1*st International Symposium on Functionally Gradient Materials*, *Japan.*
2. M. KOIZUMI 1993 *Ceramic Transactions*, *Functionally Gradient Materials* **34**, 3–10. The concept of FGM.
3. H. REISMANN and Y. LEE 1969 in *Developments in Theoretical and Applied Mechanics* (D. FREDRICK, editor), Vol. 4, 3–18. Forced motions of rectangular plates.
4. T. ROCK and E. HINTON 1974 *Earthquake Engineering & Structural Dynamics* **3**, 51–63. Free vibration and transient response of thick and thin plates using the finite element method.
5. J. N. REDDY and N. D. PHAN 1984 *Journal of Sound and Vibration* **98**, 157–170. Stability and vibration of isotropic, orthotropic and laminated plates according to a higher-order shear deformation theory.
6. A. BHIMARADDI and K. CHANDRASHEKHARA 1993 *International Journal of Solids and Structures* **30**, 1255–1268. Nonlinear vibrations of heated antisymmetric angle-ply laminated plates.
7. J. N. REDDY 1983 *International Journal of Numerical Methods in Engineering* **19**, 237–255. Dynamic (Transient) analysis of layered anisotropic composite-material plates.
8. T. KANT, V. RAVICHANDRAN, B. N. PANDYA and MALLIKARJUNA 1988 *Composite Structures* **9**, 319–342. Finite element transient dynamic analysis of isotropic and fibre reinforced composite plates using a higher-order theory.
9. K. M. LIEW, Y. XIANG and S. KITIPORNCHAI 1994 *Computers and Structures* **49**, 69–78. Transverse vibration of thick rectangular plates-IV: influence of isotropic in-plane pressure.
10. O. L. ROUFAEIL and D. J. DAWE 1982 *Journal of Sound and Vibration* **85**, 263–275. Rayleigh-Ritz vibration analysis of rectangular Mindlin plates subjected to membrane stresses.
11. A. W. LEISSA 1973 *Journal of Sound and Vibration* **31**, 257–293. The free vibration of rectangular plates.
12. F. L. LIU and K. M. LIEW 1999 *Journal of Sound and Vibration* **225**, 915–934. Analysis of vibrating thick rectangular plates with mixed boundary constraints using differential quadrature element method.
13. K. M. LIEW, Y. XIANG and S. KITIPORNCHAI 1993 *Computers and Structures* **49**, 1–29. Transverse vibration of thick rectangular plates—I: comprehensive sets of boundary conditions.
14. H. S. SHEN, J. YANG and L ZHANG 2000 *Journal of Sound and Vibration* **232**, 309–329. Dynamic response of Reissner-Mindlin plates under thermomechanical loading and resting on elastic foundations.
15. Y. TANIGAWA, T. AKAI, R. KAWAMURA and N. OKA 1996 *Journal of Thermal Stresses* **19**, 77–102. Transient heat conduction and thermal stress problems of a nonhomogeneous plate with temperature-dependent material properties.
16. J. N. REDDY and C. D. CHIN 1998 *Journal of Thermal Stresses* **21**, 593–626. Thermo-mechanical analysis of functionally graded cylinders and plates.
17. C. T. LOY, K. Y. LAM and J. N. REDDY 1999 *International Journal of Mechanical Sciences* **41**, 309–324. Vibration of functionally graded cylindrical shells.
18. S. W. GONG, K. Y. LAM and J. N. REDDY 1999 *International Journal of Impact Engineering* **22**, 397–417. The elastic response of functionally graded cylindrical shells to low-velocity impact.
19. X. Q. HE, T. Y. NG, S. SIVASHANKER and K. M. LIEW 2001 *International Journal of Solids and Structures* **38**, 1641–1655. Active control of FGM plates with integrated piezoelectric sensors and actuators.

20. G. N. PRAVEEN and J. N. REDDY 1998 *International Journal of Solids and Structures* **35**, 4457–4476. Nonlinear transient thermoelastic analysis of functionally graded ceramic-metal plates.
21. J. N. REDDY 2000 *International Journal for Numerical Methods in Engineering* **47**, 663–684. Analysis of functionally graded plates.
22. J. N. REDDY 1997 *Mechanics of Laminated Composite Plates*: *Theory and Analysis*. Boca Raton, FL: CRC Press.
23. H. S. SHEN 2002 *International Journal of Mechanical Sciences* **44**, 561–584. Nonlinear bending response of functionally graded plates subjected to transverse loads and in thermal environments.
24. H. S. SHEN 2001 *Computer Methods in Applied Mechanics and Engineering* **190**, 5377–5390. Thermal postbuckling behavior of imperfect shear deformable laminated plates with temperature-dependent properties.
25. J. YANG and L. ZHANG 2001 *Thin-Walled Structures* **38**, 195–227. Nonlinear analysis of imperfect laminated thin plates under transverse and in-plane loads and resting on an elastic foundation by a semi analytical approach.
26. J. YANG, H. S. SHEN and L. ZHANG 2001 *Composite Structures* **52**, 137–148. Nonlinear local response of foam-filled sandwich plates with laminated faces under combined transverse and in-plane loads.
27. H. DU, M. K. LIM and R. M. LIN 1994 *International Journal for Numerical Methods in Engineering* **37**, 1881–1896. Application of generalized differential quadrature method to structural problems.
28. Y. S. TOULOUKIAN 1967 *Thermophysical Properties of High Temperature Solid Materials*. New York: McMillan.